Supporting Information

Binary A_xB_{1-x} ionic alkaline pseudocapacitor system involving manganese, iron, cobalt, and nickel: formation of electroactive colloids via in-situ electric field assisted coprecipitation

Kunfeng Chen[1], Shu Yin[2,] and Dongfeng Xue[1,]**

[1]State Key Laboratory of Rare Earth Resource Utilization, Changchun Institute of Applied Chemistry, Chinese Academy of Sciences, Changchun 130022, China

[2]Institute of Multidisciplinary Research for Advanced Materials, Tohoku University, 2-1-1 Katahira, Aoba-ku, Sendai 980-8577, Japan

*E-mail: shuyin@tagen.tohoku.ac.jp; dongfeng@ciac.ac.cn

Experimental

Reagents: All chemicals were of analytical reagent grade unless otherwise stated. $MnCl_2{\cdot}4H_2O$, $FeCl_3{\cdot}6H_2O$, $CoCl_2{\cdot}6H_2O$, $NiCl_2{\cdot}6H_2O$, and KOH were supplied from Beijing Chemical Works, China. Polyvinylidene fluoride (PVDF), N-methyl-2-pyrrolidone (NMP) and carbon black were purchased from Hefei Kejing Materials Technology Co., LTD. China. Ultrapure water was used throughout the work.

Electrode preparation and test: The commercial $MnCl_2{\cdot}4H_2O$, $FeCl_3{\cdot}6H_2O$, $CoCl_2{\cdot}6H_2O$, $NiCl_2{\cdot}6H_2O$ salts were directly used without further purification. The supercapacitor electrodes were prepared by mixing 70 wt% binary salts, 20 wt% carbon black, and 10 wt% polyvinylidene fluoride (PVDF) and dissolving in N-methyl-2-pyrrolidone (NMP) solution. The binary salts consist of two kinds of salts with different molecular ratios. Briefly, the resulting slurry was spread on nickel foam current collector with an area of 1×1 cm^2. The electrodes were dried at 80 °C for 24 h, and finally pressed at 10 MPa and served as working electrode. The loading of each electrode is ~4-6 mg. Cyclic voltammetry (CV), and

galvanostatic charge-discharge measurements were obtained using an electrochemical workstation (CHI 660D, CH Instruments, Inc. Shanghai China) at designed potential range, scan rate and current density. All electrochemical experiments were carried out using a classical three-electrode configuration in 2 M KOH electrolytes. The saturated calomel electrode (SCE) electrode was used as the reference electrode, and Pt wire electrode as a counter electrode.

Characterization. To observe surface morphologies of salt electrode before and after electrochemical tests, scanning electron microscope was performed by a field-emission scanning electron microscope (FESEM, Hitachi-S4800, Japan) at acceleration voltage of 10kV. Chemical compositions of integrated electrodes were recorded using powder X-ray diffractometer (XRD, Bruker D8 Focus, Germany).

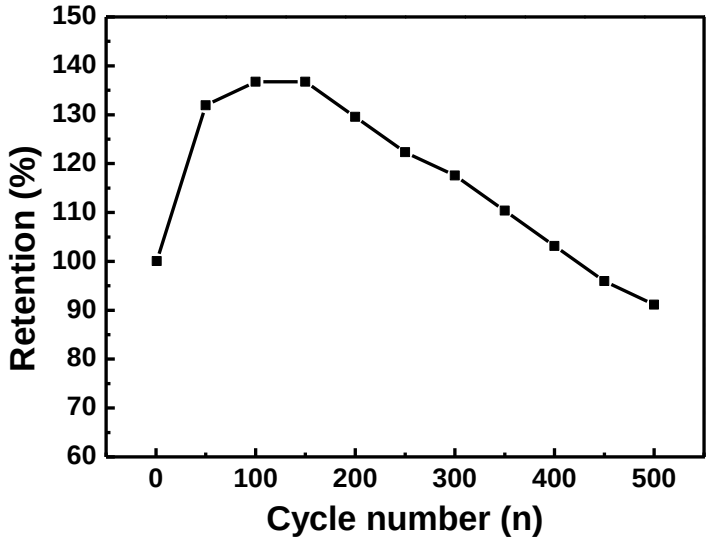

Figure S1. Cycling stability of binary $Fe_{0.7}Co_{0.3}$ electrode measured in 2M KOH electrolyte at the current density of 10 A/g and at potential range of 0-0.38 V.

Fig. S1 shows cycling stability of binary $Fe_{0.7}Co_{0.3}$ electrode measured in 2M KOH electrolyte at the high current density of 10 A/g and at potential interval of 0-0.38 V. Until

100 discharge-charge cycles, the specific capacitance of binary $Fe_{0.7}Co_{0.3}$ electrode increases, while the capacitance value decrease after 150 discharge-charge cycles. After 500 discharge-charge cycles, the 91.2 % of capacitance can be retained when compared with the initial value. At the initial discharge-charge cycles, binary transition metal salts were in situ transformed into electroactive hydroxides or metal oxides colloids by the electric field assisted chemical coprecipitation. Because the electroactive component was gradually increased, the specific capacitance of binary salt electrode also increased. Then, the high active component began to lose part of its electroactivity at high discharge-charge current rate, leading to the decrease of specific capacitance. The fluctuation in specific capacitance was due to the competition between the high electroactivity and high stability.

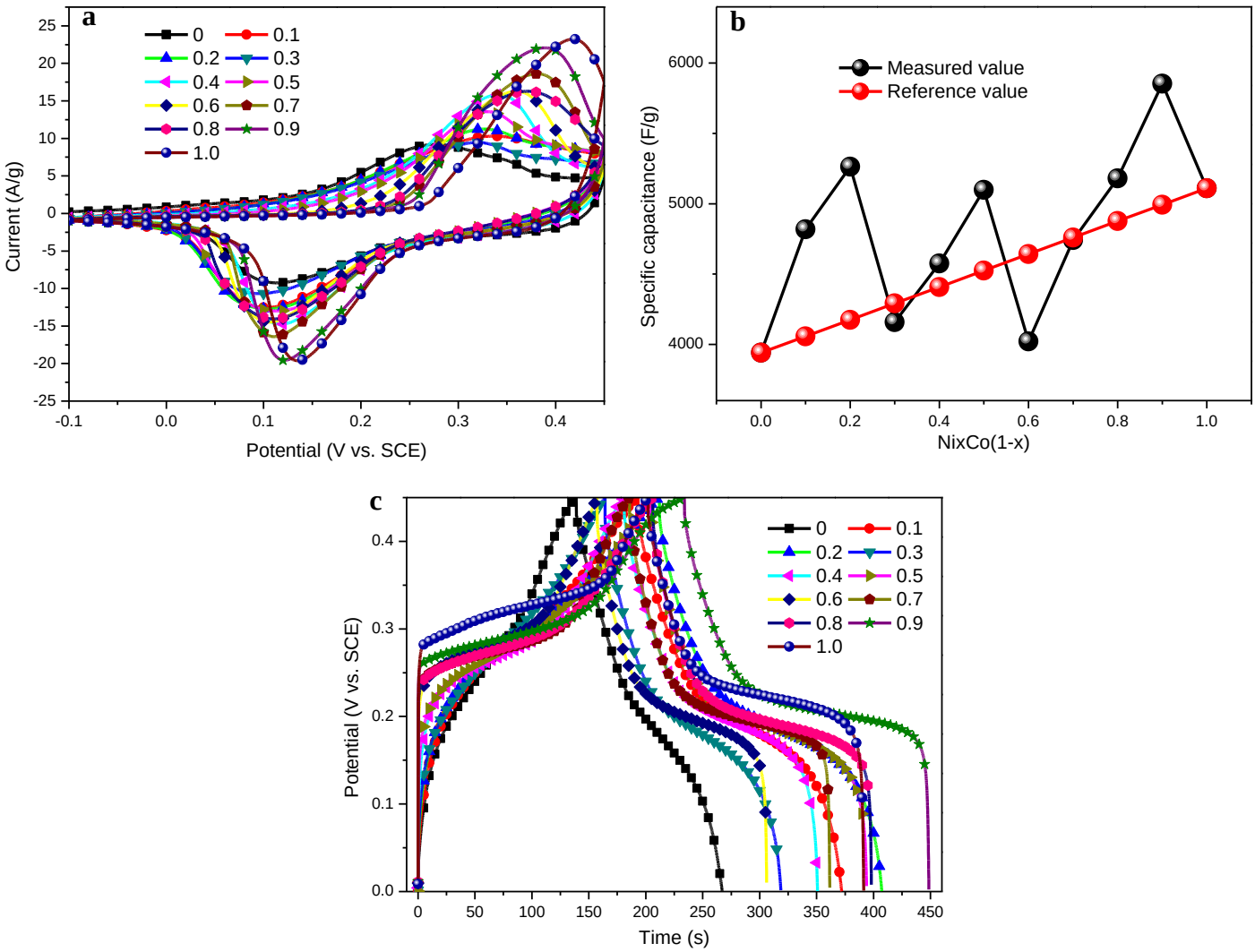

Figure S2. Electrochemical performances of Ni_xCo_{1-x} ($0 \le x \le 1$) salt electrodes in 2M KOH electrolyte. (a) CV curves (current density versus potential) at rate of 5 mV/s and potential range of -0.1-0.45 V. A pair of redox peaks is present at the CV curves, showing the pseudocapacitive characteristic. (b) Variation of specific capacitance as a function of ratio of x ($0 \le x \le 1$) at current density of 3 A/g. (c) The charge-discharge curves (time versus potential) measured at current density of 3 A/g.

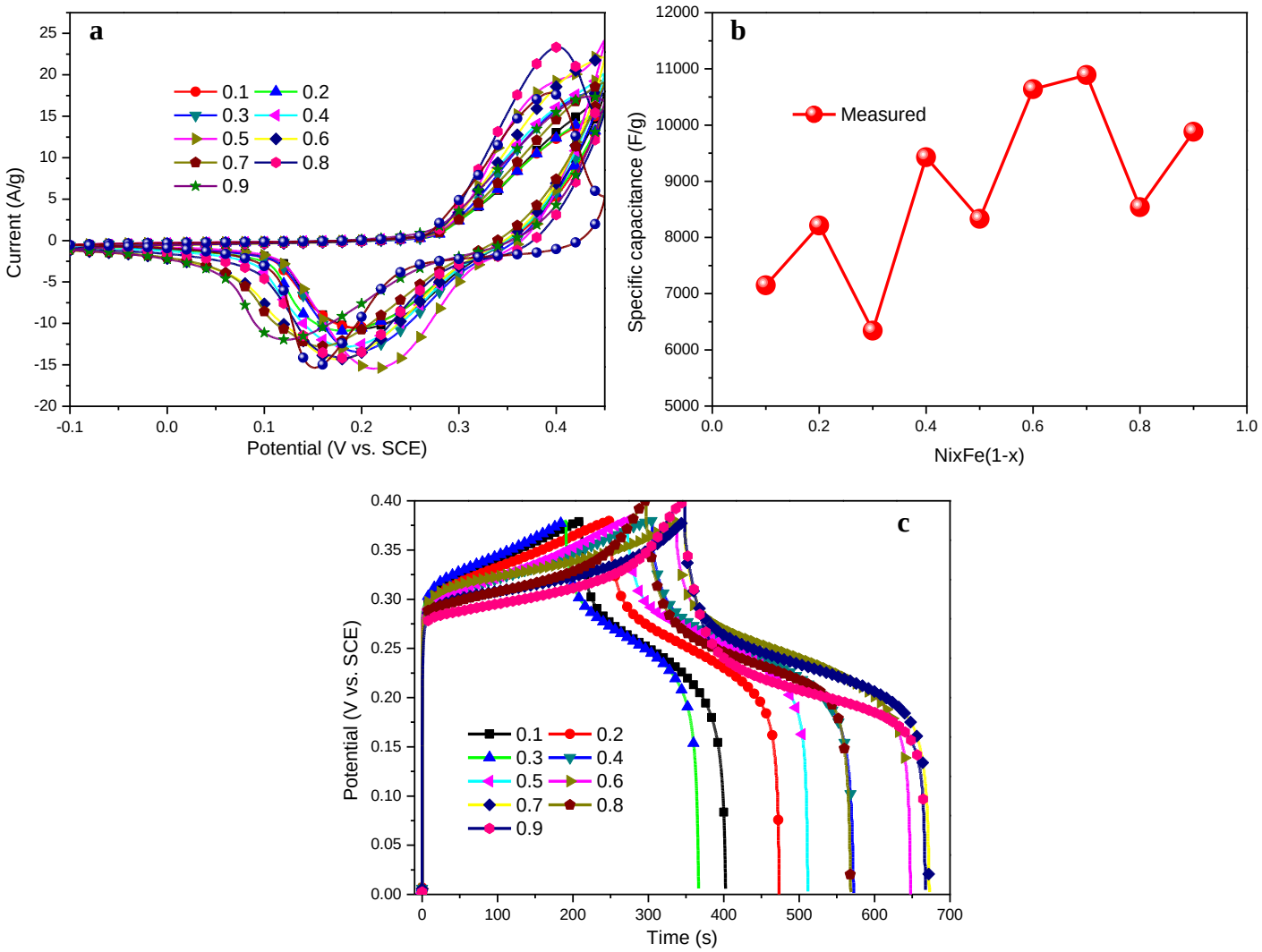

Figure S3. Electrochemical performances of Ni_xFe_{1-x} ($0.1 \leq x \leq 0.9$) salts electrodes in 2M KOH electrolyte. (a) CV curves (current density versus potential) at rate of 3 mV/s and potential range of -0.1-0.45 V. A pair of redox peaks is present at the CV curves, showing the pseudocapacitive characteristic. (b) Variation of specific capacitance as a function of ratio of x ($0.1 \leq x \leq 0.9$) at current density of 3 A/g. (c) The charge-discharge curves (time versus potential) measured at current density of 3 A/g.

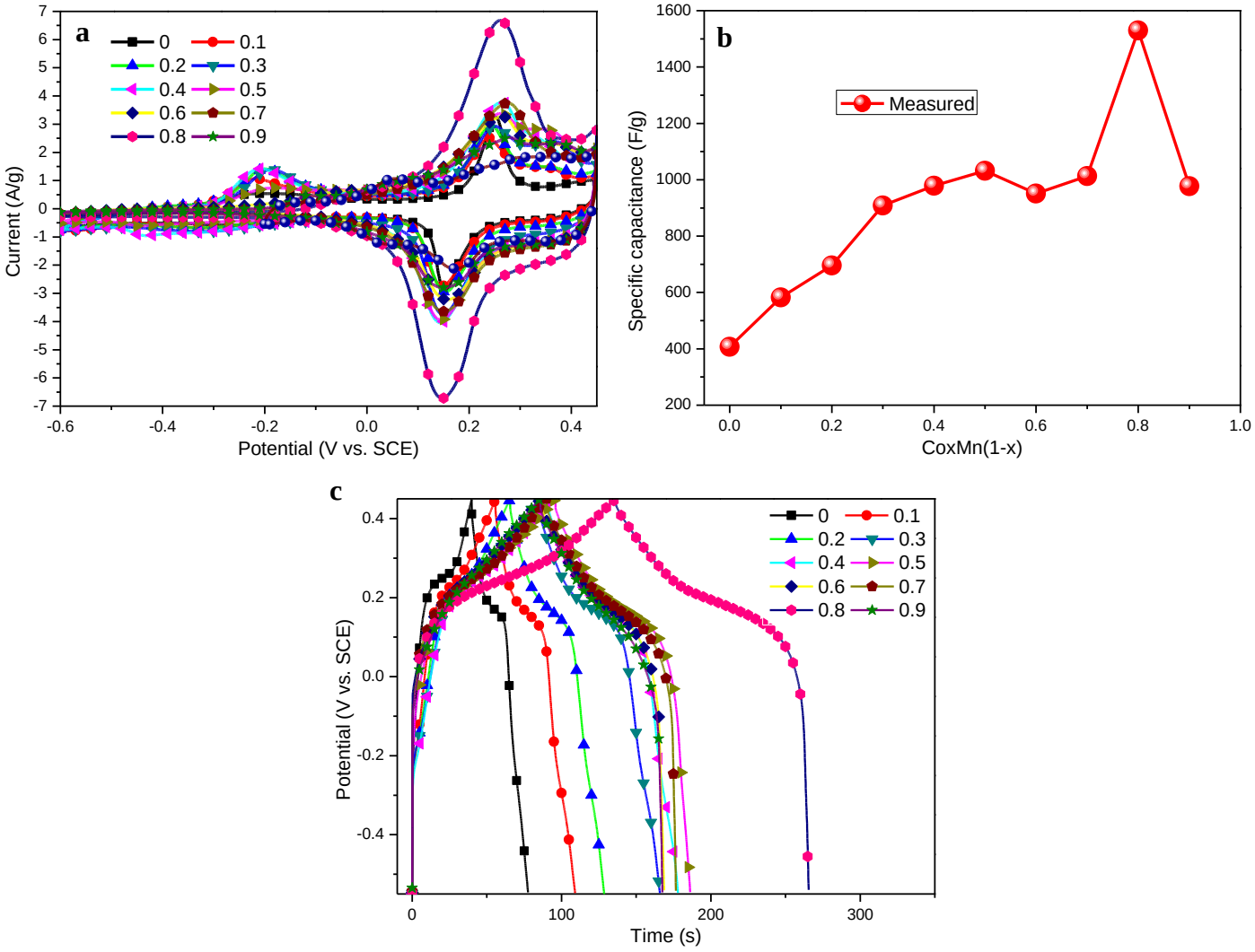

Figure S4. Electrochemical performances of Co_xMn_{1-x} ($0 \le x \le 0.9$) salts electrodes in 2M KOH electrolyte. (a) CV curves (current density versus potential) at rate of 3 mV/s and potential range of -0.6-0.45 V. A pair of redox peaks is present at the CV curves, showing the pseudocapacitive characteristic. (b) Variation of specific capacitance as a function of the ratio of x ($0 \le x \le 0.9$) at current density of 3 A/g. (c) The charge-discharge curves (time versus potential) measured at current density of 3 A/g.

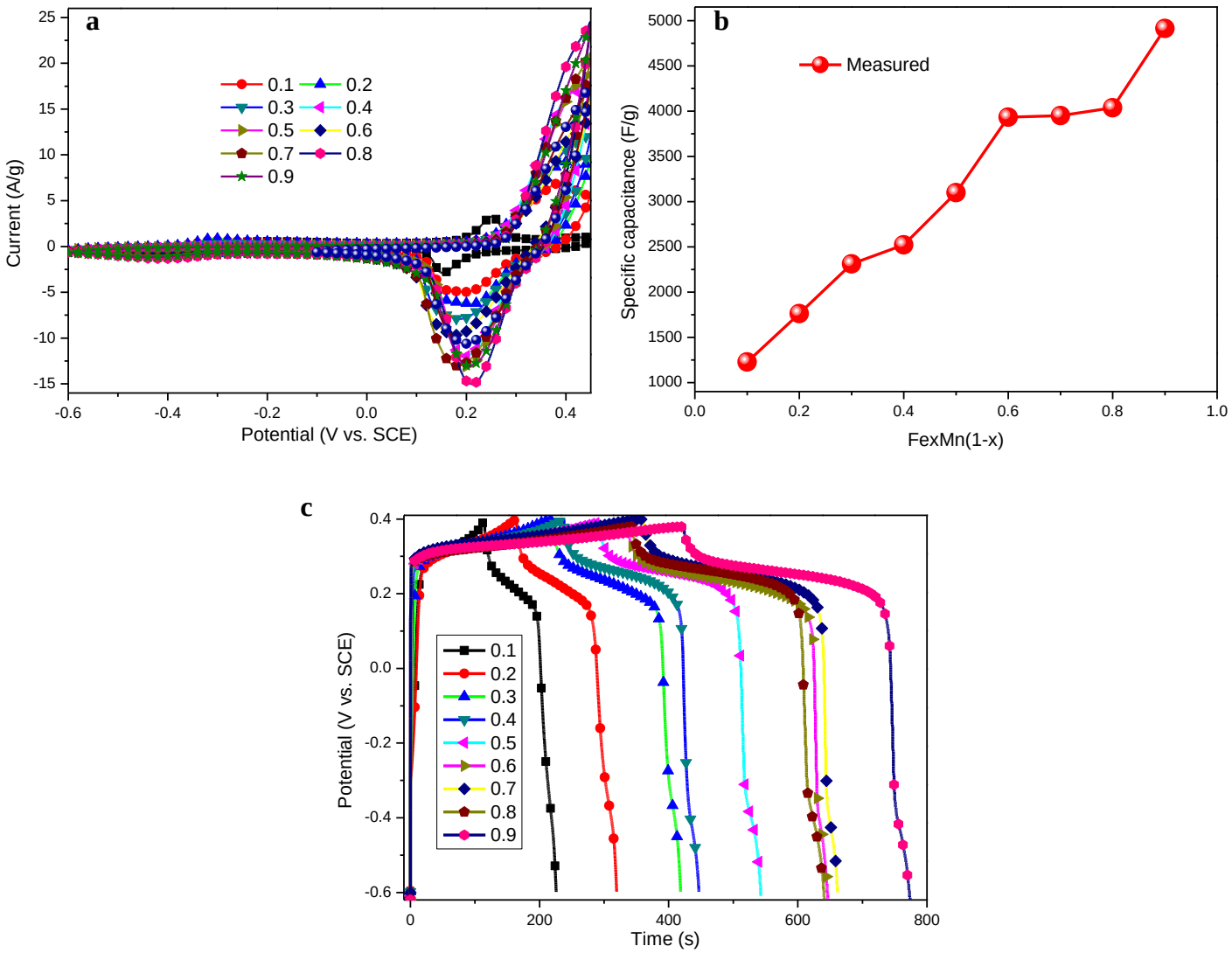

Figure S5. Electrochemical performances of Fe_xMn_{1-x} ($0 \leq x \leq 0.9$) salts electrodes in 2M KOH electrolyte. (a) CV curves (current density versus potential) at rate of 3 mV/s and potential range of -0.6-0.45 V. A pair of redox peaks is present at the CV curves, showing the pseudocapacitive characteristic. (b) Variation of specific capacitance as a function of ratio of x ($0 \leq x \leq 0.9$) at current density of 3 A/g. (c) The charge-discharge curves (time versus potential) measured at current density of 3 A/g.

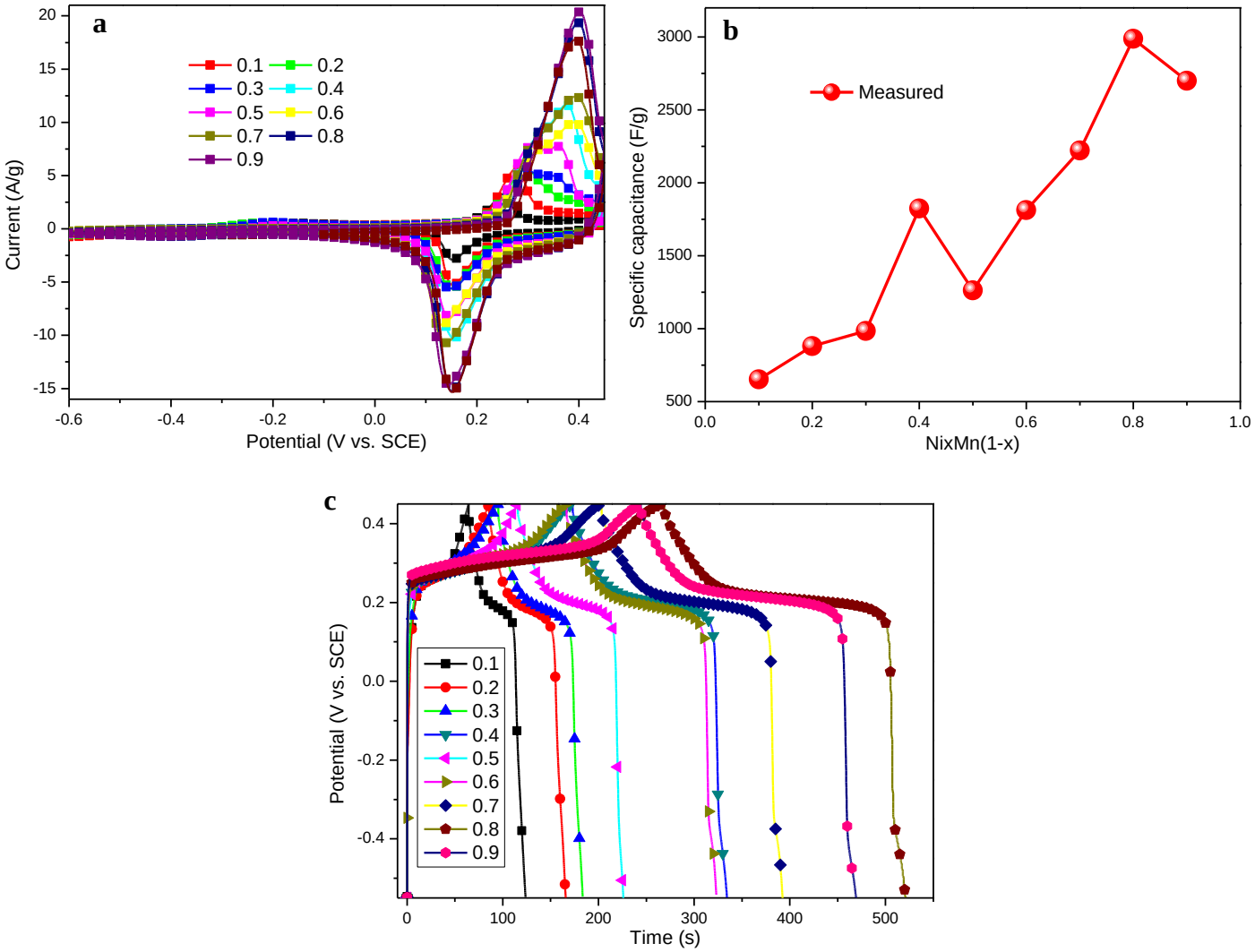

Figure S6. Electrochemical performances of $Ni_xMn_{(1-x)}$ salts electrodes in 2M KOH electrolyte. (a) CV curves (current density versus potential) at rate of 3 mV/s and potential range of -0.6-0.45 V. A pair of redox peaks is present at the CV curves, showing the pseudocapacitive characteristic. (b) Variation of specific capacitance as a function of ratio of x ($0 \leq x \leq 0.9$) at current density of 3 A/g. (c) The charge-discharge curves (time versus potential) measured at current density of 3 A/g.

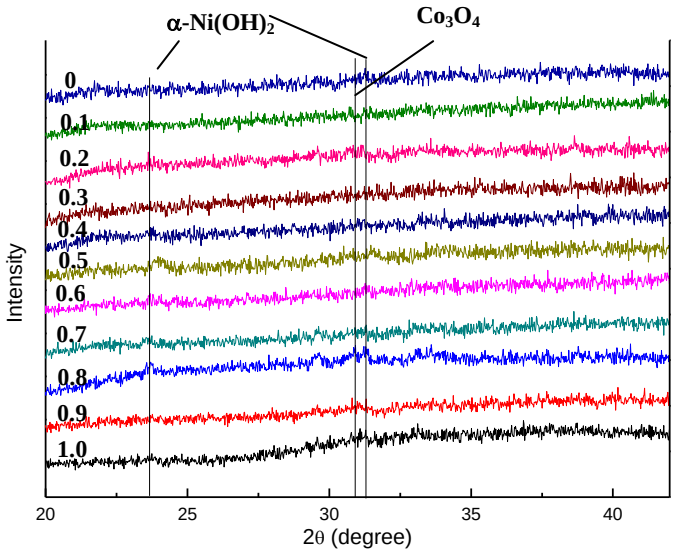

Figure S7. XRD patterns of Ni_xFe_{1-x} salt electrodes after electrochemical measurement in 2 M KOH electrolyte. α-$Ni(OH)_2$, and Co_3O_4 phases are indicated in figure, which are consistent with the standard JCPDS No. 22-444 for α-$Ni(OH)_2$, 80-1545 for Co_3O_4.

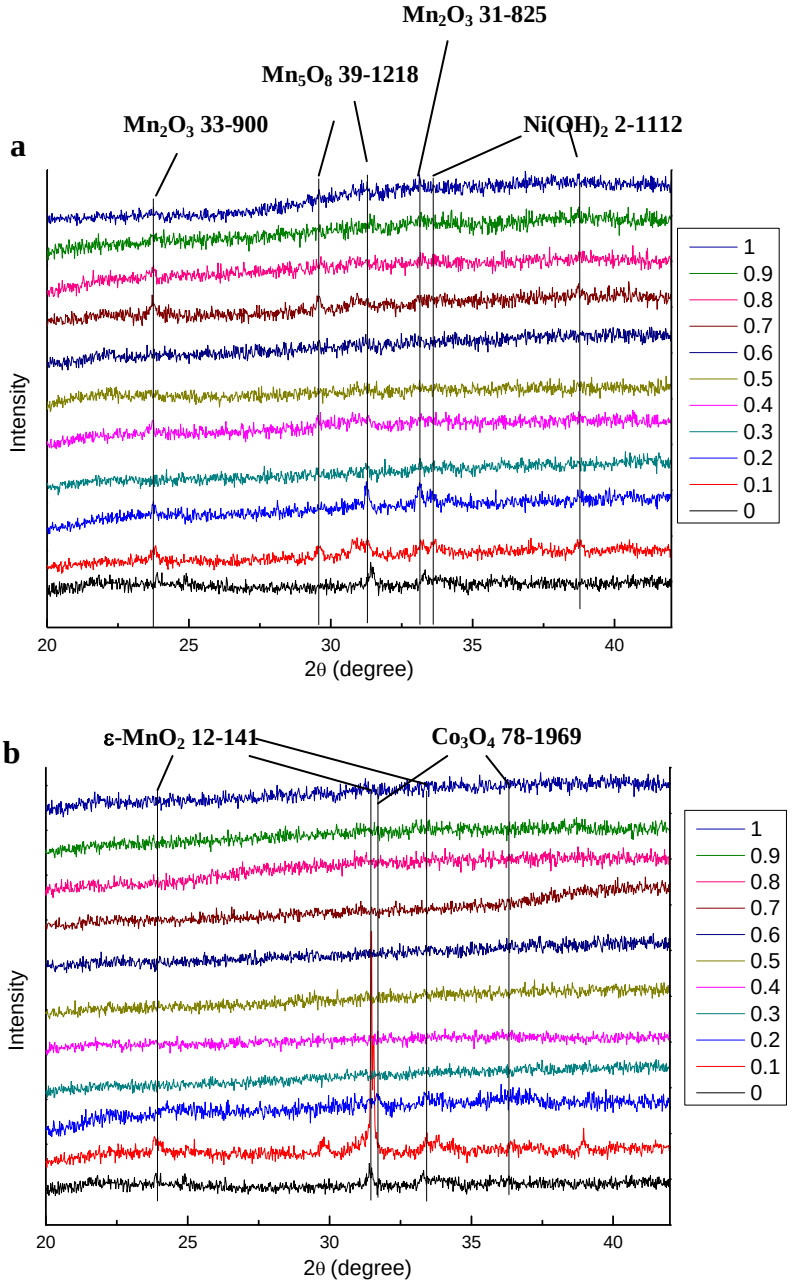

Figure S8. XRD patterns of Ni_xMn_{1-x} (a) and Co_xMn_{1-x} (b) salts electrodes after electrochemical measurement in 2 M KOH electrolyte. As-synthesized phases are indicated in figures, which are consistent with the standard JCPDS shown in figures.

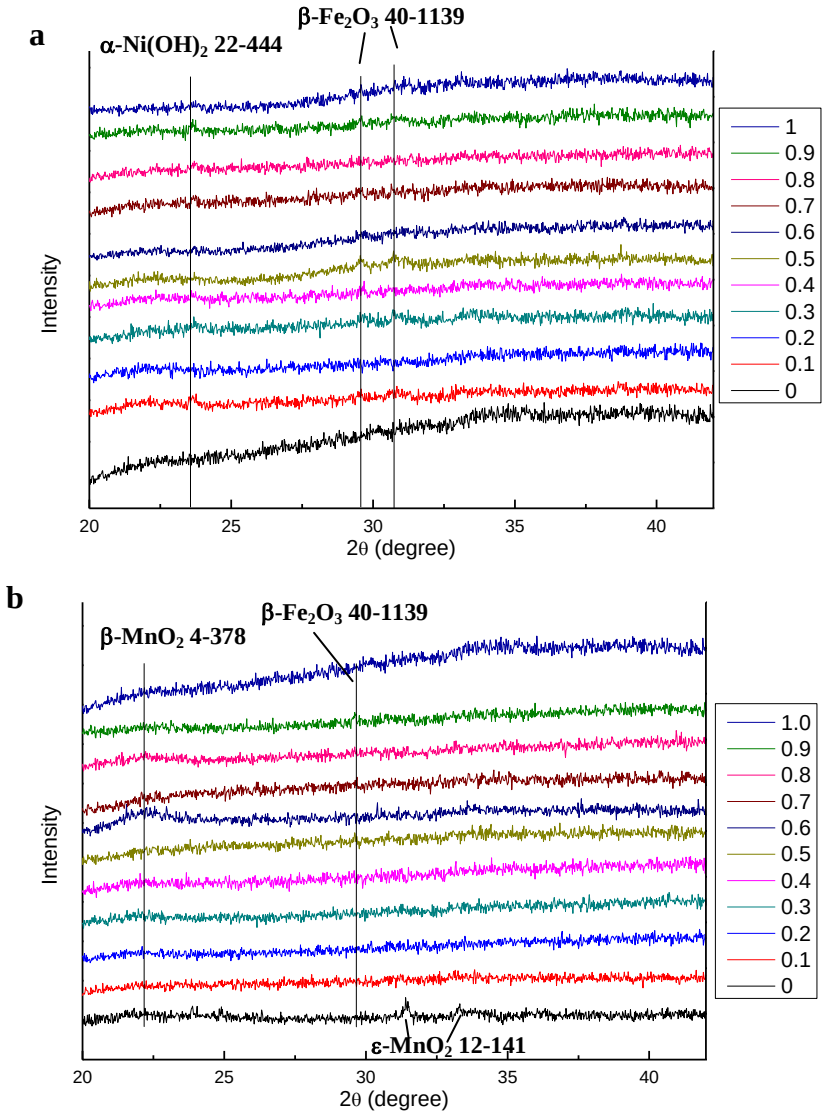

Figure S9. XRD patterns of Ni_xFe_{1-x} (a) and Fe_xMn_{1-x} (b) salts electrodes after electrochemical measurement in 2 M KOH electrolyte. As-obtained phases are indicated in figures, which are consistent with the standard JCPDS shown in figures.

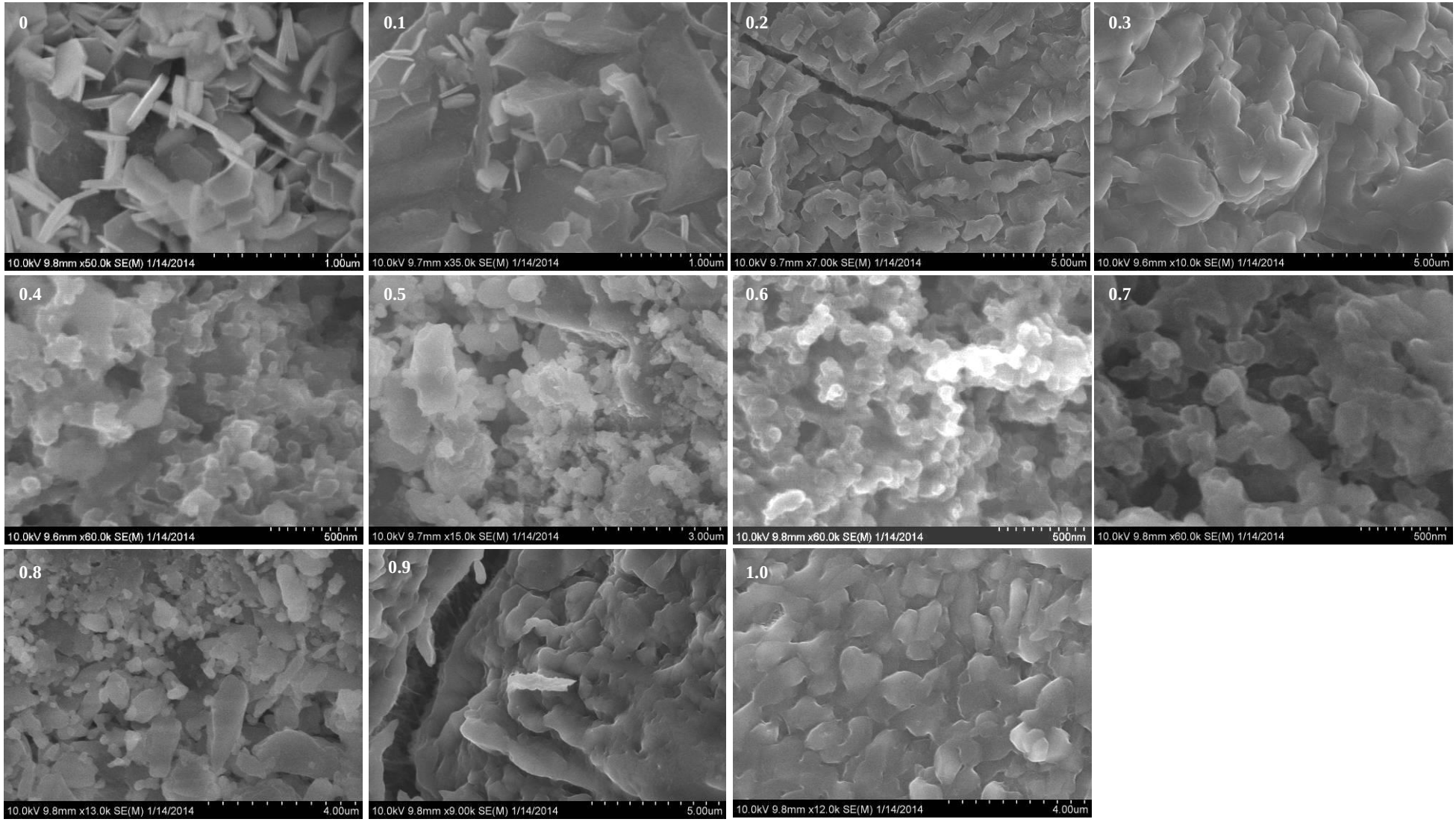

Figure S10. SEM images of Ni_xCo_{1-x} salts electrodes after electrochemical measurement in 2 M KOH electrolyte. The values of x are shown in figures.